Dokuz Eylül Üniversitesi Mühendislik Fakültesi Fen ve Mühendislik Dergisi
Dokuz Eylul University Faculty of Engineering Journal of Science and Engineering

Preparation and characterization of magnetic featured supported heterogeneous catalysts
Manyetik özellikli desteklenmiş heterojen katalizörlerin hazırlanması ve karakterizasyonu

Yıldıray Aldemir[1] , **Elif Ant Bursalı[2]** , **Mürüvvet Yurdakoc[2],***

[1]Dokuz Eylül University, Graduate School of Natural and Applied Sciences, Department of Chemistry, Izmir,TURKEY.
[2]Dokuz Eylül University, Faculty of Sciences, Department of Chemistry, 35390 Izmir,TURKEY
Sorumlu Yazar / Corresponding Author *: m.yurdakoc@deu.edu.tr

Abstract

Magnesium ferrite nanoparticles containing organic or inorganic support materials were prepared as heterogeneous catalysts. The characterization of the catalysts was performed by X-ray powder diffraction (XRD), Fourier transform infrared spectroscopy (FTIR), emission scanning electronic microscope/energy dispersive spectroscopy (SEM/EDS). Magnetic properties of the catalysts were determined by a vibrating sample magnetometer (VSM). Specific surface area and pore size distribution of the catalysts were obtained from nitrogen adsorption-desorption data at 77K by Brunauer-Emmett-Teller (BET) method.
Keywords: Heterogeneous catalysts, Nanoparticles, Magnesium ferrite

Öz

Organik veya inorganik destek malzemeleri içeren magnezyum ferrit nanoparçacıklı heterojen katalizörler hazırlanmıştır. Katalizörlerin karakterizasyonu X-ışını toz kırınımı (XRD), Fourier dönüşümlü kızılötesi spektroskopi (FTIR), taramalı elektron mikroskop/enerji dağıtıcı spektroskopi (SEM/EDS) ile gerçekleştirilmiştir. Katalizörlerin manyetik özellikleri titreşimli örnek manyetometresi (VSM) ile belirlenmiştir. Katalizörlerin özgül yüzey alanı ve gözenek boyutu dağılımı, 77K'de azot adsorpsiyon-desorpsiyon verilerinden Brunauer-Emmett-Teller (BET) yöntemi ile elde edilmiştir.
Anahtar Kelimeler: Heterojen katalizörler, Nanoparçacıklar, Magnezyum ferrit

1. Introduction

Magnetic nanoparticles have gained considerable interest due to having diverse chemical and physical properties in various technological applications [1-4] such as catalysis [5-9], drug delivery [10, 11], adsorption [12-15], sensors [16, 17] and biomedical applications [18-20].

Magnetic nanoparticles with tunable catalytic activities are attractive catalysts since they can be separated from the reaction medium after magnetization by an external magnet.

The cubic spinel ferrites represent an important class of magnetic nanoparticles. Nano magnesium ferrite ($MgFe_2O_4$) with a cubic structure of inverse spinel type is a member of spinel ferrites. It is a soft magnetic n-type semiconducting material which has good photoelectrical properties, low saturation magnetization, high resistivity, uniform and reproducible characteristics [3, 4].

Also clays are important in industrial raw materials such as catalyst and catalyst supports. Clays are the combination of one or more clay minerals including traces of metal oxides and organic materials that are naturally find in rocks or soils [21]. Organoclays are organically modified clay minerals with large surface areas. An organophilic surface is generated by exchanging the original interlayer cations with organic species such as primary aliphatic amine salts and alkylammonium ions [22].

Magnesium ferrite nanoparticles containing organic or inorganic support materials are of great interest in the preparation of heterogeneous catalysts. In this study natural Enez/Edirne bentonite (B), organo-bentonite (HB/CTAB) and nano aluminum oxide (NPs-Al_2O_3) supported nano spheres of $MgFe_2O_4$ were prepared by co-precipitation method [20].

All prepared catalysts were characterized by XRD, FTIR, SEM/EDS, and VSM methods and compared with each other. Specific surface areas and adsorption-desorption isotherms of the catalysts were determined by BET method.
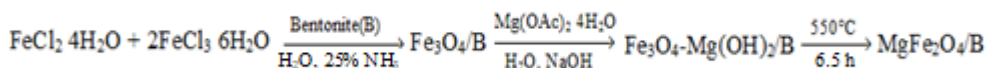
2. Material and Method

Iron(II) chloride tetrahydrate ($FeCl_2.4H_2O$) (Merck), Iron(III) chloride hexahydrate ($FeCl_3.6H_2O$) (Merck), aqueous ammonia (NH_3) (Carlo Erba), magnesium acetate tetrahydrate ($Mg(OAc)_2.4H_2O$) (Merck) and sodium hydroxide (NaOH) (Merck) were used for the preparation of magnesium ferrite nano spheres.

Natural Enez/Edirne bentonite (B), organo bentonite (HB / CTAB) [23] and nano aluminum oxide (NPs-Al_2O_3) (Aldrich) were used as support materials for the preparation of catalysts. All other chemicals used were of analytical reagent grade and used without further purification. The water used throughout the study was deionized. A Heildolph MR 3001 model magnetic shaker and a Carbolite model muffle furnace were used during the experiments.

2.1. Preparation of the nano spheres of magnesium ferrite with different support materials

The catalysts were prepared by co-precipitation method because of its simplicity and having a good product distribution. So, 30 mL solution of $FeCl_2.4H_2O$ (368 mg, 1.85 mmol) and $FeCl_3.6H_2O$ (1g, 3.7 mmol) was prepared with deionized water under a nitrogen atmosphere in order to avoid oxidation of magnetic nanoparticles. The mixture was slowly added to the flask containing 1g support material (B, HB/CTAB or NPs-Al_2O_3) in the same atmosphere. After 10 min, aqueous solution of 10 mL 25% NH_3 was added to the mixture at a constant dropping rate (2mL/min) at room temperature and was stirred at 700 rpm for 20 min. 10 mL solution of $Mg(OAc)_2.4H_2O$ (750 mg, 3.5 mmol) in deionized water was added drop wise to the suspension. $Mg(OH)_2$ was allowed to precipitate with the controlled addition of 1 M NaOH to the solution. The precipitate formed was filtered, washed several times with deionized water, dried in an oven and was calcined at 550 °C for 6.5 h. The synthesized catalysts were named as $MgFe_2O_4/B$, $MgFe_2O_4/HB$-CTAB, $MgFe_2O_4/NPs$-Al_2O_3, respectively.

Hypothetically proposed reaction scheme for preparation of $MgFe_2O_4/B$ was given as an example in Scheme 1[20].

$$FeCl_2 \cdot 4H_2O + 2FeCl_3 \cdot 6H_2O \xrightarrow[H_2O,\ 25\%\ NH_3]{Bentonite(B)} Fe_3O_4/B \xrightarrow[H_2O,\ NaOH]{Mg(OAc)_2 \cdot 4H_2O} Fe_3O_4\text{-}Mg(OH)_2/B \xrightarrow[6.5\ h]{550°C} MgFe_2O_4/B$$

Scheme 1. Reaction scheme for preparation of $MgFe_2O_4/B$.

2.2. Characterization of the catalysts

The X-ray diffraction patterns (XRD) of the catalysts were recorded in a Rigaku - Rint 2200/PC (Ultima 3) X-Ray diffractometer using Cu K_α radiation in the 2θ range of 10-90° with a scanning rate of 0.4 degree/min.

Fourier transform infrared spectroscopy (FTIR) spectra of the catalysts were recorded with a Perkin Elmer Spectrum BX-II Model Fourier Transform IR spectrometer using KBr pellets in the range of 4000 and 400 cm^{-1}, at a resolution of 4 cm^{-1} and averages of 50 scans.

Morphological analyses of catalysts were performed with an emission scanning electronic microscope (SEM), FEI Quanta FEG 250 operated at an acceleration voltage of 5 kV. Also, elemental distribution was determined by energy dispersive spectroscopy (EDS) working in conjunction with the SEM.

The magnetization measurements were carried out by using a vibrating sample magnetometer (VSM) (Cryogenic Limited PPMS) with a magnetic field range up to ±5 T at room temperature.

The specific surface area of catalysts determined according to the Brunauer-Emmett-Teller (BET) method after N_2 adsorption-desorption at 77 K by using Quantachrome Corporation, Autosorb-6.
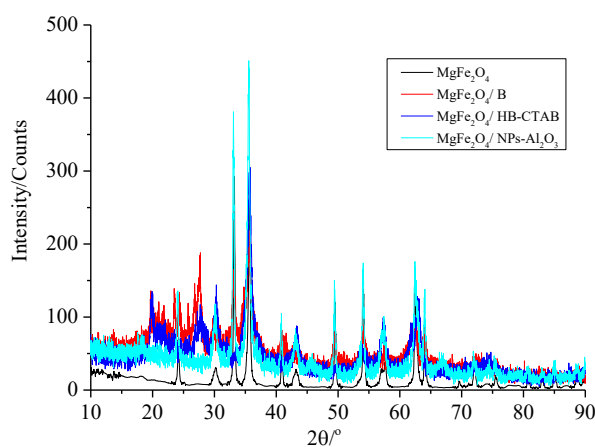
3. Results

3.1. XRD analysis

The X-ray powder diffraction pattern of $MgFe_2O_4$ (Figure 1) was evaluated according to JCPDS 17-0464 and Hematite, α-Fe_2O_3 phase has been observed as impurity [24].
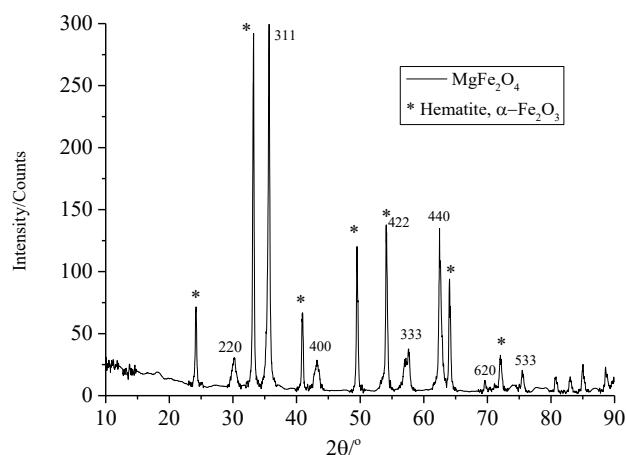
Figure 1. XRD pattern of $MgFe_2O_4$

Figure 2. XRD patterns of $MgFe_2O_4$, $MgFe_2O_4/B$, $MgFe_2O_4/HB$-CTAB and $MgFe_2O_4/NPs$-Al_2O_3

As can be seen from Figure 2 the structure of active ingredient, $MgFe_2O_4$, was protected. The intensities of the signals of $MgFe_2O_4/B$, $MgFe_2O_4/HB$-CTAB and $MgFe_2O_4/NPs$-Al_2O_3 were increased in comparison with the signals of $MgFe_2O_4$.

Also by using XRD data, the crystallite sizes of the $MgFe_2O_4$, $MgFe_2O_4/B$, $MgFe_2O_4/HB$-CTAB and $MgFe_2O_4$ / NPs-Al_2O_3 catalysts were calculated as 31, 15, 9 and 27 nm, respectively, which indicated nano sized catalysts.

3.2. FTIR analysis

The FTIR spectra of the samples in the range of 4000-400 cm^{-1} were shown in Figure 3. The spectra of $MgFe_2O_4$ showed absorption bands around 3380 cm^{-1} and 1637 cm^{-1}, which were characteristic stretching and bending vibrations of hydroxylate (O–H) remain at the calcination temperature of 550 °C, respectively [25].

The small bands lying at 2924 cm^{-1} and 1046 cm^{-1} were characteristic of C-H stretching and bending modes, respectively. The absorption band observed at 2364 cm^{-1} could be assigned to atmospheric CO_2 [26].

The characteristic absorption bands appeared at 567 cm^{-1} and 460 cm^{-1} were corresponding to stretching vibration of metal–oxygen bonds at tetrahedral and octahedral sites respectively and they were responsible for the formation of $MgFe_2O_4$ structure [20, 27,

28]. According to the spectra of $MgFe_2O_4$ a significant decrease in intensities and increase in frequencies of the bands occurred in the spectra of $MgFe_2O_4/NPsAl_2O_3$.

Besides, the intensities of the bands observed in the spectra of B were increased in the spectra of $MgFe_2O_4/B$ by the effect of $MgFe_2O_4$. In comparison with the spectra of $MgFe_2O_4$ and HB-CTAB, the intensities of all bands were significantly reduced and some bands could not be observed in the spectrum of $MgFe_2O_4/HB$-CTAB.

### 3.3. SEM analysis

SEM and EDS analysis were applied to all samples and their support materials. Images of the surface of the samples at 25000x magnification were shown in Figure 4 and the EDS results of the samples were given in Table 1.

In the SEM image of $MgFe_2O_4$ (Figure 4g), any aggregate was observed. On the other hand, as can be seen from Figure 4 that for $MgFe_2O_4/HB$-CTAB and $MgFe_2O_4/NPs$-Al_2O_3 (Figure 4d and f) catalysts, aggregations as a part in the images were observed. In the case of $MgFe_2O_4/HB$-CTAB maximum degree of aggregation was observed with spacings between the aggregates. In Figure 4b, for $MgFe_2O_4/B$, formation of an aggregation was not seen and when compared with B (Figure 4a) due to the small particles it may be considered that the effect of $MgFe_2O_4$ on the structure was more than bentonite.
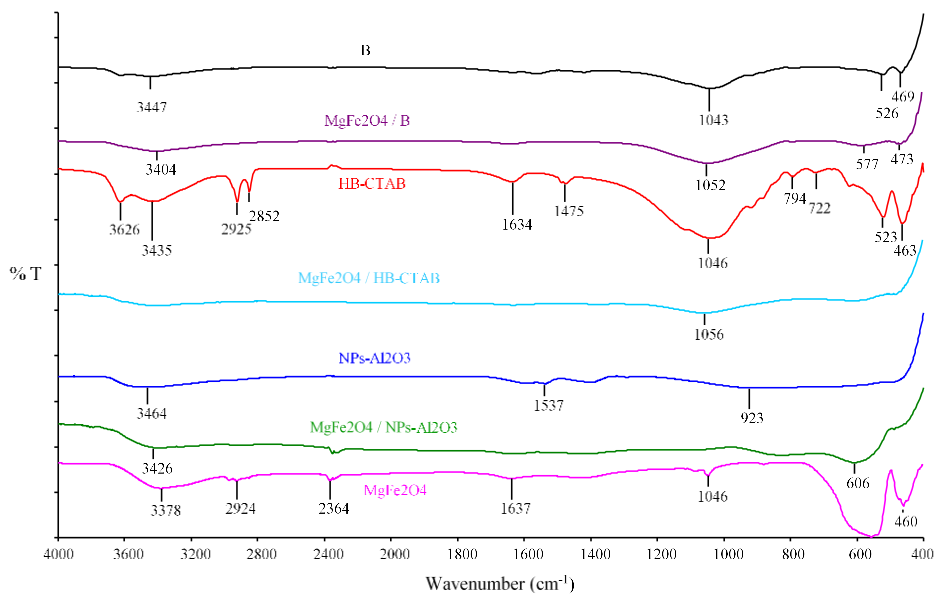
Figure 3. FTIR spectra of the samples
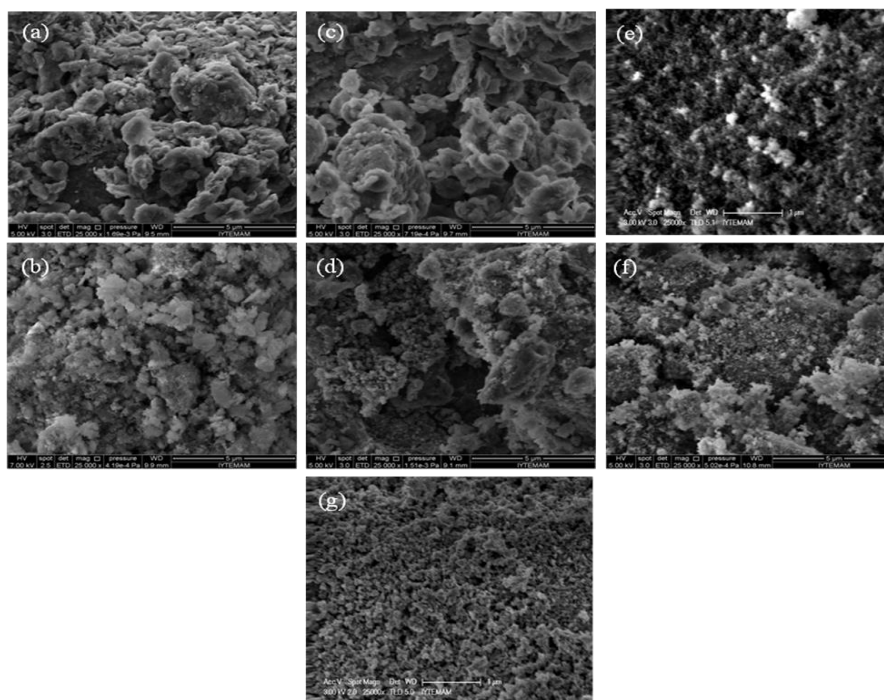
Figure 4. SEM images of the surface of samples at 25000x magnification. (a) B, (b) $MgFe_2O_4$/B, (c) HB-CTAB, (d) $MgFe_2O_4$/HB-CTAB, (e) NPs-Al_2O_3, (f) $MgFe_2O_4$/NPs-Al_2O_3 and (g) $MgFe_2O_4$

Table 1. EDS results of the samples (w %)

Sample	Mg	Fe	Al	C	O	Si
$MgFe_2O_4$	6.92	76.34	-	1.85	14.89	-
$MgFe_2O_4/B$	4.43	22.16	3.47	17.81	42.15	9.98
$MgFe_2O_4/HB$-CTAB	4.70	21.01	3.63	15.15	45.72	9.79
$MgFe_2O_4 / NPs$-Al_2O_3	**3.71**	29.59	10.59	15.69	40.42	-

C% values seen in Table 1 could be explained by carbon strips used in sample preparation of SEM analysis for $MgFe_2O_4$, by calcite and carbonate structures of natural bentonite for $MgFe_2O_4/B$ and by the solute of commercial NPs-Al_2O_3 (20% isopropanol) for $MgFe_2O_4/NPs$-Al_2O_3.

3.4. VSM analysis

The magnetization behaviors of the samples were evaluated using a VSM, as shown in Figure 5. It is clear that the samples exhibit S-shape curves and hysteresis were not observed which was typical for superparamagnetic behavior [17, 29-31].

Having magnetic properties provide to be easily and quickly separated from the suspensions for the obtained nanoparticles.

The saturation magnetization (M_s) values of $MgFe_2O_4/HB$-CTAB, $MgFe_2O_4/NPs$-Al_2O_3, $MgFe_2O_4/B$ and $MgFe_2O_4$ were 11.8, 8.7, 2.1 and 7.8 emu/g at room temperature, respectively.

$MgFe_2O_4/HB$-CTAB and $MgFe_2O_4/NPs$-Al_2O_3 had higher M_s values than that of $MgFe_2O_4$, where $MgFe_2O_4/B$ had a lower value. The value of M_s was related to the crystallinity of the nanoparticles [31].
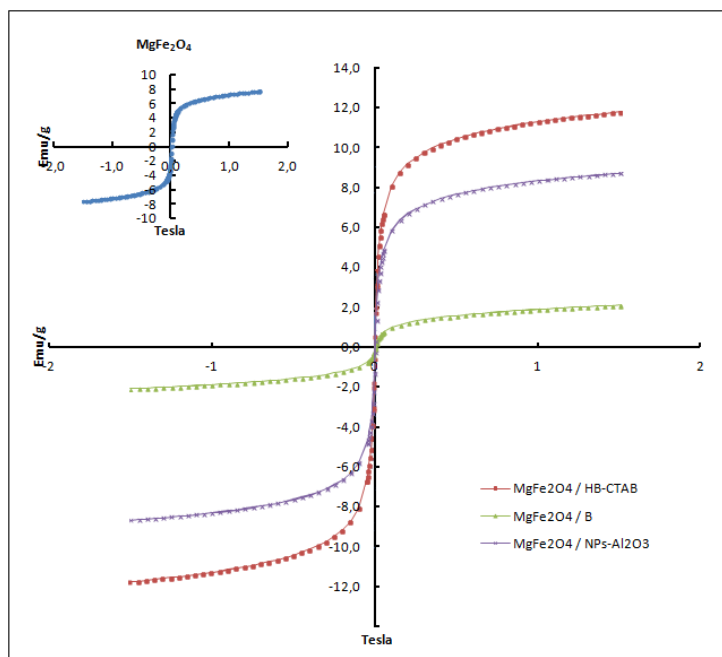
Figure 5. Magnetization curves of the samples at room temperature

3.5. BET Analysis

BET multi point specific surface areas (S_{BET}(m^2/g)), BJH pore volumes (Vp (cm^3/g)) and BJH pore diameters (Å) of B, HB-CTAB, NPs-Al_2O_3, $MgFe_2O_4$, $MgFe_2O_4$/B, $MgFe_2O_4$/HB-CTAB and $MgFe_2O_4$ / NPs-Al_2O_3 after N_2 adsorption-desorption at 77 K were represented in Table 2.

When the surface area values of B and HB-CTAB were compared, it was observed that the surface areas decreased with the acid activation of B and the diffusion of CTAB between the layers and may be being partially filling the pores. The proximity of the values of B and $MgFe_2O_4$/B to each other showed that $MgFe_2O_4$ has not diffused between the layers or porous structure of bentonite but probably dispersed onto the surface. The highest surface area of $MgFe_2O_4$/HB-CTAB among the catalysts was inferred from the increase in pore volume and average pore diameter which was probably due to the penetration of HB-CTAB into the layers of $MgFe_2O_4$. This may

be due to the treatment of acid activated bentonite (HB) or B with CTAB will increase the distance between the layers of HB, namely B which can be confirmed with the XRD results. This extra space may be resulted an increase in the specific surface area of the $MgFe_2O_4$/HB-CTAB.

Besides, it was observed that more N_2 was adsorbed because of the increase in pore volume and average pore diameter, and by the increase of monolayer capacity, the specific surface area was also increased.

In the case of $MgFe_2O_4$/NPs-Al_2O_3, a significant decrease in the specific surface area value was observed as compared with NPs-Al_2O_3. This may be due to the filling of the pores with of $MgFe_2O_4$ particles.

As can be seen from Figure 6, the BET isotherms indicated a non-porous or mesoporous structure with Type S, Type II, according to IUPAC classification [32].

Table 2. S_{BET}, Pore Volume (V_p) and Pore Diameter of B, HB-CTAB, NPs-Al_2O_3, $MgFe_2O_4$, $MgFe_2O_4$/B, $MgFe_2O_4$/HB-CTAB and $MgFe_2O_4$ / NPs-Al_2O_3

Sample	S_{BET} m²/g	(BJH)* Pore Volume, V_p cm³/g	(BJH) Method Pore Diameter Å
B	65	0.1300	41.0
HB-CTAB	25	0.0774	14.5
NPs-Al_2O_3	98	0.6928	305
$MgFe_2O_4$	27	0.2365	299
$MgFe_2O_4$/B	67	0.2176	38.6
$MgFe_2O_4$/HB-CTAB	101	0.2160	30.8
$MgFe_2O_4$ / NPs-Al_2O_3	66	0.4278	291

*The method of Barrett, Joyner, and Halenda (BJH) is a procedure for calculating pore size distributions from experimental isotherms using the Kelvin model of pore filling. It applies only to the mesopore and small macropore size range.
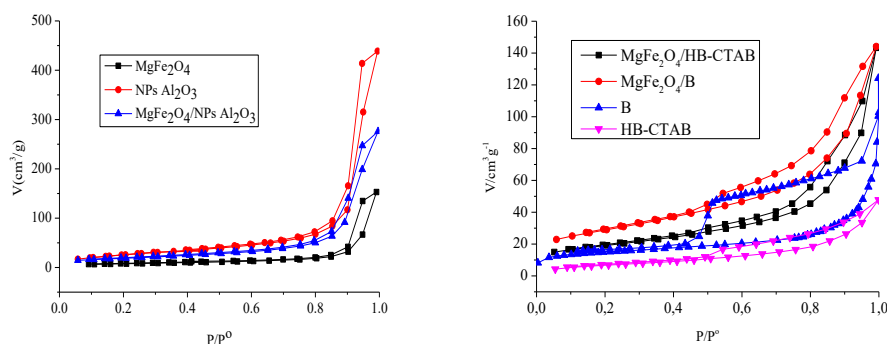
Figure 6. Multi point BET adsorption-desorption isotherms of N_2 at 77 K for B, HB-CTAB, NPs-Al_2O_3, $MgFe_2O_4$, $MgFe_2O_4$/B, $MgFe_2O_4$/HB-CTAB and $MgFe_2O_4$ / NPs-Al_2O_3

4. Discussion and Conclusion

$MgFe_2O_4$/B, $MgFe_2O_4$/HB-CTAB and $MgFe_2O_4$/NPs-Al_2O_3 catalysts were synthesized and the calculated crystallite sizes of these catalysts indicated nano sized particles according to XRD datas. The characteristic bands of magnesium ferrite were observed in all of the FTIR spectra. Samples exhibit S-shape curves in VSM analysis and hysteresis was not observed which was typical for superparamagnetic behavior. The saturation magnetization (M_s) values of $MgFe_2O_4$/HB-CTAB, $MgFe_2O_4$/NPs-Al_2O_3, $MgFe_2O_4$/B and $MgFe_2O_4$ were obtained as 11.8, 8.7, 2.1 and 7.8 emu/g at room temperature, respectively. Also BET isotherms indicated a non-porous or mesoporous structure with Type S, Type II, according to

144

IUPAC classification. As a result, the synthesized magnetic catalysts may be used as photocatalysts and noncomposite adsorbents by interacting with light sensitive materials and organic monomers in later stages. In addition, the magnetic property can provide advantages in terms of time and application by reducing the catalyst loss compared to conventional methods such as filtration and precipitation in separation processes.

References

[1] Xie, X., Shen, W., 2009. Morphology control of cobalt oxide nanocrystals for promoting their catalytic performance, Nanoscale1, 1, 50-60. DOI: 10.1039/B9NR00155G

[2] Song, S., Wang, H., Song, A., Dong, S., Hao, J., 2014. Sponge phase producing porous CeO_2 for catalytic oxidation of CO, Chemistry–A European Journal, 20(29), 9063-9072. DOI: 10.1002/chem. 201304836

[3] Xie, P., Chen, L., Ma, Z., Huang, C., Huang, Z., Yue, Y., Hua, W., Tang, Y., Gao, Z., 2014. Hydrothermal conversion of Fe_2O_3/SiO_2 spheres into Fe_2O_3/Silicalite-1 nanowires: Synthesis, characterization, and catalytic properties. Microporous and mesoporous materials, 200, 52-60. DOI: 10.1016/j.micromeso. 2014.08.020

[4] Hong, S. S., 2005. Catalytic removal of carbon particulates over $MgFe_2O_4$ catalysts, Reaction Kinetics and Catalysis Letters, 84(2), 311-317. DOI:10.1007/s11144-005-0224-3

[5] Ma, N., Yue, Y., Hua, W., Gao, Z., 2003. Selective oxidation of styrene over nanosized spinel-type $MgxFe_{3-x}O_4$ complex oxide catalysts, Applied Catalysis A: General, 251(1), 39-47. DOI: 10.1016/S0926-860X(03)00306-5

[6] Liu, J., Qiao, S. Z., Chen, J. S., Lou, X. W. D., Xing, X., Lu, G. Q. M., 2011. Yolk/shell nanoparticles: new platforms for nanoreactors, drug delivery and lithium-ion batteries, Chemical Communications, 47(47), 12578-12591. DOI: 10.1039/C1CC13658E

[7] Li, F., Zhu, Y., Wang, Y., 2014. Dual-responsive drug delivery system with real time tunable release behavior, Microporous and mesoporous materials, 200, 46-51. DOI: 10.1016/j.micromeso. 2014.07.060

[8] Hao, J., Yang, W., Zhang, Z., Pan, S., Lu, B., Ke, X., Zhang, B., Tang, J., 2013. Hierarchical flower-like $Co_{3-x}Fe_xO_4$ ferrite hollow spheres: facile synthesis and catalysis in the degradation of methylene blue, Nanoscale, 5(7), 3078-3082. DOI: 10.1039/ C3NR00041A

[9] Yu, X. Y., Meng, Q. Q., Luo, T., Jia, Y., Sun, B., Li, Q. X., Liu, J. H., Huang, X. J., 2013. Facet-dependent electrochemical properties of Co_3O_4 nanocrystals toward heavy metal ions, Scientific reports, 3, 2886. DOI: 10.1038/srep02886

[10] Wang, B., Wu, H., Yu, L., Xu, R., Lim, T. T., Lou, X. W., 2012. Template-free formation of uniform urchin-like α-FeOOH hollow spheres with superior capability for water treatment, Advanced Materials, 24, 1111-1116. DOI: 10.1002/adma.201104599

[11] Wen, Z., Zhang, Y., Dai, C., Chen, B., Guo, S., Yu, H., Wu, D., 2014. Synthesis of ordered mesoporous iron manganese bimetal oxides for arsenic removal from aqueous solutions, Microporous and mesoporous materials, 200, 235-244. DOI: 10.1016/j.micromeso. 2014.08.049

[12] Lai, X., Li, J., Korgel, B. A., Dong, Z., Li, Z., Su, F., Du, J., Wang, D., 2011. General synthesis and gas-sensing properties of multiple-shell metal oxide hollow microspheres, Angewandte Chemie International Edition, 50(12), 2738-2741. DOI: 10.1002/anie. 201004900

[13] Shao, M., Xu, X., Han, J., Zhao, J., Shi, W., Kong, X., Wei, M., Evans, D.G., Duan, X., 2011. Magnetic-field-assisted assembly of layered double hydroxide/metal porphyrin ultrathin films and their application for glucose sensors, Langmuir, 27(13), 8233-8240. DOI: 10.1021/la201521w

[14] Chan, A., Orme, R. P., Fricker, R. A., Roach, P., 2013. Remote and local control of stimuli responsive materials for therapeutic applications, Advanced drug delivery reviews, 65(4), 497-514. DOI: 10.1016/j.addr.2012. 07.007

[15] Laurent, S., Dutz, S., Häfeli, U. O., Mahmoudi, M., 2011. Magnetic fluid hyperthermia: focus on superparamagnetic iron oxide nanoparticles, Advances in colloid and interface science, 166(1-2), 8-23. DOI: 10.1016/j.cis.2011.04.003

[16] Maehara, T., Konishi, K., Kamimori, T., Aono, H., Hirazawa, H., Naohara, T., Nomura, S., Kikkawa, H., Watanabe, Y., Kawachi, K., 2005. Selection of ferrite powder for thermal coagulation therapy with alternating magnetic field, Journal of materials science, 40(1), 135-138. DOI: 10.1007/s10853-005-5698-x

[17] Nonkumwong, J., Ananta, S., Jantaratana, P., Phumying, S., Maensiri, S., Srisombat, L., 2015. Phase formation, morphology and magnetic properties of $MgFe_2O_4$ nanoparticles synthesized by hydrothermal technique. Journal of Magnetism and Magnetic Materials, 381, 226-234. DOI: 10.1016/j.jmmm. 2015.01.001

[18] Kang, D., Yu, X., Ge, M., Song, W., 2015. One-step fabrication and characterization of hierarchical $MgFe_2O_4$ microspheres and their application for lead removal, Microporous and Mesoporous Materials, 207, 170-178. DOI: 10.1016/j.micromeso.2015.01.023

[19] Ilhan, S., Izotova, S. G., Komlev, A. A., 2015. Synthesis and characterization of $MgFe_2O_4$ nanoparticles prepared by hydrothermal decomposition of co-precipitated magnesium and iron hydroxides, Ceramics International, 41(1), 577-585. DOI: 10.1016/j.ceramint.2014.08.106

[20] Sheykhan, M., Mohammadnejad, H., Akbari, J., Heydari, A., 2012. Superparamagnetic magnesium ferrite nanoparticles: a magnetically reusable and clean heterogeneous catalyst, Tetrahedron Letters, 53(24), 2959-2964. DOI: 10.1016/j.tetlet.2012.03.069

[21] Önal, M., 2006. Physicochemical properties of bentonites: an overview, Commun. Fac. Sci. Univ. Ank. Series B, 52, 7-21.

[22] Bardziński, P. J., 2014. On the impact of intermolecular interactions between the quaternary ammonium ions on interlayer spacing of quat-intercalated montmorillonite: A molecular mechanics and ab-initio study, Applied clay science, 95, 323-339. DOI: 10.1016/j.clay.2014.04.035

[23] Akçay, G., Yurdakoç, M. K., 1999. Nonyl-and dodecylamines intercalated bentonite and illite from Turkey, Turkish Journal of Chemistry, 23(1), 105-114.

[24] Cross, W. B., Affleck, L., Kuznetsov, M. V., Parkin, I. P., Pankhurst, Q. A., 1999. Self-propagating high-temperature synthesis of ferrites MFe_2O_4 (M= Mg, Ba, Co, Ni, Cu, Zn); reactions in an external magnetic field, Journal of Materials Chemistry, 9(10), 2545-2552. DOI: 10.1039/A904431K

[25] Huang, Y., Tang, Y., Wang, J., Chen, Q., 2006. Synthesis of $MgFe_2O_4$ nanocrystallites under mild conditions, Materials Chemistry and Physics, 97(2-3), 394-397, DOI: 10.1016/j.matchemphys.2005.08.035

[26] Kang, D., Yu, X., Ge, M., Song, W., 2015. One-step fabrication and characterization of hierarchical $MgFe_2O_4$ microspheres and their application for lead removal, Microporous and Mesoporous Materials, 207, 170-178. DOI: 10.1016/j.micromeso.2015.01.023

[27] Khot, V. M., Salunkhe, A. B., Thorat, N. D., Phadatare, M. R., Pawar, S. H., 2013. Induction heating studies of combustion synthesized $MgFe_2O_4$ nanoparticles for hyperthermia applications, Journal of Magnetism and Magnetic Materials, 332, 48-51. DOI: 10.1016/j.jmmm.2012.12.010

[28] Hoque, S. M., Hakim, M. A., Mamun, A., Akhter, S., Hasan, M. T., Paul, D. P., Chattopadhayay, K., 2011. Study of the bulk magnetic and electrical properties of $MgFe_2O_4$ synthesized by chemical method, Materials Sciences and Applications, 2(11), 1564. DOI: 10.4236/msa.2011.211209

[29] Wang, L., Ren, J., Wang, Y., Liu, X., Wang, Y., 2010. Controlled synthesis of magnetic spinel-type nickel ferrite nanoparticles by the interface reaction and hydrothermal crystallization, Journal of alloys and compounds, 490(1-2), 656-660. DOI: 10.1016/ j.jallcom.2009.10.131

[30] Yu, B. Y., Kwak, S. Y., 2011. Self-assembled mesoporous Co and Ni-ferrite spherical clusters consisting of spinel nanocrystals prepared using a template-free approach, Dalton Transactions, 40(39), 9989-9998. DOI: 10.1039/C1DT10650C

[31] Nejati, K., Zabihi, R., 2012. Preparation and magnetic properties of nano size nickel ferrite particles using hydrothermal method, Chemistry Central Journal, 6(1), 23-28. DOI: 10.1186/1752-153X-6-23

[32] Sing, K. S., Everett, D.H., Haul, R.A.W., Moscou, L., Pierotti, R.A., Rouquerol, J., Siemieniewska, T., 1985. Reporting physisorption data for gas/solid systems with special reference to the determination of surface area and porosity (Recommendations 1984), Pure and applied chemistry, 57(4), 603-619.